ULK1-mediated phosphorylation of ATG16L1 promotes xenophagy, but destabilises the ATG16L1 Crohn's mutant

Reham M. Alsaadi[#1], Truc T. Losier[#1], Wensheng Tian[1], Anne Jackson[2], Zhihao Guo[1], David C. Rubinsztein[2,3], Ryan C. Russell[1,4]*.

[1]Department of Cellular and Molecular Medicine, University of Ottawa, 451 Smyth Road, Ottawa, Ontario K1H 8M5, Canada.

[2]Department of Medical Genetics, University of Cambridge, Cambridge Institute for Medical Research, The Keith Peters Building, Cambridge Biomedical Campus, Hills Road, Cambridge CB2 0XY, UK.

[3]UK Dementia Research Institute, Cambridge Biomedical Campus, Hills Road, Cambridge CB2 0XY, UK

[4]University of Ottawa Center for Infection, Immunity and Inflammation

[#]denotes equal contribution

*Address for correspondence: 451 Smyth Rd, Ottawa, Ontario, K1H 8M5, Canada. E-mail: ryan.russell@uottawa.ca

Running title: ULK1-ATG16L1 signalling: friend or foe?

Keywords: ULK1, ATG16L1, Crohn's Disease, Autophagy, Caspase

Abstract

Autophagy is a highly regulated catabolic pathway that is potently induced by stressors including starvation and infection. An essential component of the autophagy pathway is an ATG16L1-containing E3-like enzyme, which is responsible for lipidating LC3B and driving autophagosome formation. ATG16L1 polymorphisms have been linked to the development of Crohn's disease (CD) and phosphorylation of CD-associated ATG16L1 T300A (caATG16L1) has been hypothesised to contribute to cleavage and autophagy dysfunction. Here we show that ULK1 kinase directly phosphorylates ATG16L1 in response to infection and starvation. Phosphorylated ATG16L1 localises to the site of internalised bacteria and stable cell lines harbouring a phospho-dead mutant of ATG16L1 have impaired xenophagy, indicating a role for ATG16L1 phosphorylation in the promotion of anti-bacterial autophagy. In contrast to wild-type ATG16L1, ULK1-mediated phosphorylation of caATG16L1 drives its destabilization in response to stress. In summary, our results show that ATG16L1 is a novel target of ULK1 kinase and that ULK1-signalling to ATG16L1 is a double-edged sword, enhancing the function of the wildtype ATG16L1, but promoting degradation of caATG16L1.

Introduction

Macroautophagy (hereafter referred to as autophagy) is a cellular degradative process capable of degrading a vast array of substrates including cytoplasm, organelles, aggregated macromolecules, and pathogens[1]. Autophagic cargo is first sequestered by the formation a double membraned vesicle called an autophagosome, which matures into a degradative vesicle after fusion with lysosomes. Autophagosome formation is driven by a set of autophagy-related (ATG) genes, which include a protein kinase (Unc 51-like kinase 1; ULK1), a lipid kinase (vacuolar protein sorting 34; VPS34), and a trimeric E3-like enzyme (ATG5-ATG12/ATG16L1)[1]. These enzymes are all required for autophagy initiation and are tightly regulated by upstream stress-sensitive signalling. One of the best characterised upstream regulators of the autophagy pathway is mTORC1, which potently inhibits autophagy induction through direct phosphorylation of the ULK1 and VPS34 kinase complexes[2-5]. mTORC1 activity is repressed, thereby allowing autophagy induction, in response to a myriad of stressors including nutrient or cytokine starvation, reactive oxygen species, or infection[6-8].

Mammals have two homologues of the yeast ATG1, ULK1 and ULK2, which are largely functionally redundant for autophagy induction[9]. Under basal conditions, mTORC1-mediated phosphorylation represses ULK1 activity; however, starvation releases this inhibitory phosphorylation and upregulates ULK1[2]. Activated ULK1 then phosphorylates several components of the pro-autophagic ATG14-containing VPS34 complexes[10-12]. Autophagic VPS34 complexes are recruited to the phagophore where they phosphorylate phosphatidylinositol (PtdIns) to produce phosphatidylinositol(3)phosphate (PtdIns(3)P)[13]. PtdIns(3)P functions as a platform bridging downstream components like the ATG16L1 complex to promote autophagosome formation. Additionally, mTORC1 has been shown to directly mediate the activity of VPS34 complexes, thereby allowing a tight regulation of autophagy initiation in response to stresses[3]. Downstream of VPS34, ATG16L1 forms a trimeric complex with ATG5 and ATG12. ATG16L1 is the subunit responsible for recruiting the E3-like enzyme to the phagophore[1,14]. ATG12 acts to recruit microtubule-associated protein 1 light chain 3 (LC3) to the expanding autophagosomal membrane and ATG5 catalyzes the conjugation of the ubiquitin-like LC3 to phosphatidylethanolamine in membranes of nascent autophagosomes, thereby driving their development.

Activation of anti-bacterial autophagy (hereafter referred to as xenophagy) involves these 3-key enzymes in the autophagy pathway, but also requires xenophagy-specific proteins involved in pathogen-sensing that signal to the autophagy machinery during infection[8]. For instance, galectin-8 detects damaged *Salmonella*-containing vacuoles (SCV) and subsequently activates xenophagy through

recruitment of the autophagy receptor NDP52[15]. Immunity related GTPase M (IRGM) has been shown to act as a scaffold bringing together ULK1, Beclin-1-containing VPS34 complexes, and ATG16L1 to promote xenophagy initiation[16]. In addition to IRGM, ATG16L1-containing enzyme is also regulated by activation of intracellular (NOD2) sensors of bacterial peptidoglycan, where NOD2 binds ATG16L1 recruiting the LC3-lipidating enzyme to the site of bacterial infection[17].

Interestingly, several of the proteins involved in xenophagy induction (ATG16L1 and IRGM) and pathogen detection (NOD2 and TLR4) have been linked to Crohn's disease (CD), but are not found in the related chronic inflammatory bowel disease ulcerative colitis (UC)[18]. Genome-wide association studies have linked a non-synonymous single nucleotide polymorphism (SNP) in ATG16L1 that substitutes threonine 300 for alanine with an increased susceptibility for CD[19]. Molecular characterization of the CD-associated ATG16L1 (caATG16L1) has shown that stresses such as starvation or pathogen infection enhance the susceptibility of caATG16L1 to caspase-mediated cleavage[20-23]. Enhanced cleavage of caATG16L1 has been shown to lead to an increase in inflammatory cytokine secretion and a decrease in xenophagy, which are thought to contribute to CD[21,24-26]. Interestingly, a recent study has found that IκB kinase subunit IKKα is capable of phosphorylating ATG16L1 on Serine 278 (S278), which regulates the sensitivity of caATG16L1 to caspase cleavage[24]. The caspase cleavage site on ATG16L1 lies in between the S278 phosphorylation site and the T300A Crohn's SNP. This raises the interesting possibility that phosphorylation of ATG16L1 in response to infection leads to inappropriate cleavage if the site is in close proximity to the T300A mutation. ATG16L1 contains several conserved serine/threonine residues proximal to T300, which may also be phosphorylated and may potentially regulate ATG16L1 function. However, it remains to be seen what effect phosphorylation has on wild-type ATG16L1 and if other stressors or kinases regulate ATG16L1 phosphorylation.

Results

ATG16L1 is phosphorylated by ULK1/2

Starvation has been described to trigger caspase-mediated cleavage of ATG16L1 containing a common amino acid substitution (T300A)[21]. However, IKKα has not been implicated in starvation-induced autophagy. Interestingly, ATG16L1 has been shown to bind FIP200, an essential co-factor of the ULK1 kinase complex. The interaction of ATG16L1 with FIP200 has been shown to be involved in regulating ATG16L1 localization in autophagy induction[27,28]. Therefore, we hypothesised that ULK1/2, the only protein kinases in the autophagy pathway, may phosphorylate ATG16L1 under starvation. To

test this hypothesis we performed an *in vitro* kinase assay using either purified ULK1 or ULK2 with recombinant ATG16L1 as substrate. We found that both ULK1 and ULK2 were capable of phosphorylating ATG16L1 *in vitro* (Fig. 1A). In order to narrow down the site of phosphorylation we repeated the kinase assay using truncations of ATG16L1. We found that the truncation mutant lacking amino acids 254-294 was a very poor substrate for ULK1, indicating that the primary site(s) of ULK1-mediated phosphorylation are located in this region (Fig. 1B). Amino acids 254-294 are serine/threonine rich, containing 10 conserved residues (Fig. 1C). Therefore, to identify the residue(s) that are phosphorylated by ULK1 in this region we repeated the kinase assay on full length ATG16L1 and performed mass spectrometry analysis. Our results revealed a single high confidence phosphorylation site on serine 278 (Fig. EV1A and marked in green in Fig. 1C) and another of slightly lower confidence on serine 287 (Fig. EV1A and marked in grey in Fig. 1C), both of which map to the region of ATG16L1 we previously identified as required for ULK1-mediated phosphorylation (Fig. 1B). Peptide coverage in the mass spectrometry was 80% across the whole protein and only two S/T residues were missed in the putative 254-294 region. To confirm the major site(s) of phosphorylation on ATG16L1 we mutated S278 and S287 singly in the full length protein and performed another *in vitro* ULK1 kinase assay. Interestingly, we observed a significant loss of ULK1-mediated phosphorylation in the S278A mutant and little reduction in the S287A mutant (Fig. 1D). This indicates that the major site of phosphorylation on ATG16L1 is S278, which is the same residue previously identified as a site for IKKα–mediated phosphorylation[24]. Next, we created phospho-specific antibodies against S278 or S287 of ATG16L1 and tested its specificity by co-transfection of wild-type or mutant ULK1 and ATG16L1. Excitingly, we observed that ULK1 phosphorylates ATG16L1 on S278 in cells and that our antibody was specific to the phosphorylated form of the protein with little to no signal against ATG16L1 (S278A) or wild-type ATG16L1 cotransfected with kinase-dead ULK1 (Fig. 1E). Despite good specificity for our S287 antibody (Fig. EV1B, EV1C) we observed that the lower probability site obtained by mass spectrometry, S287, was not phosphorylated in an ULK1-dependent manner (Fig. 1E). Collectively, these results show that ATG16L1 is a direct target of ULK1 and that the primary site of phosphorylation is S278.

ULK1 is required for phosphorylation of ATG16L1 and xenophagy induction

We next sought to determine if ULK1 regulated ATG16L1 phosphorylation endogenously and whether this signalling was responsive to starvation. ULK1/2 wild-type or ULK1/2 double knockout (dKO) cells were starved for amino acids, either with amino acid-free DMEM or HBSS, followed by analysis of pATG16L1 levels by western blot of whole cell extracts. Starvation potently inhibits mTORC1-

signalling, as demonstrated by loss of S6K phosphorylation, which is a prerequisite for ULK1 activation. Importantly, we observed that starvation resulted in a clear increase in endogenous ATG16L1 phosphorylation only in cells containing ULK1 (Fig. 2A, EV2A, lanes 1-6). We found that ablation of ULK1-mediated phosphorylation of ATG16L1 had no effect on the stability of the ATG16L1/5-12 complex (Fig. EV2B). Notably, our phospho-antibody only recognises the slower migrating ATG16L1β isoform and is observed as a single band. As IKKα was previously described to phosphorylate ATG16L1 on S278 under infection we also tested the requirement for IKKα in starvation-induced ATG16L1 phosphorylation. However, we observed that IKKα-deficiency had no detectable effect on starvation-induced ATG16L1 phosphorylation (Fig. 2A, lanes 7-9). This is perhaps expected as IKKα has no known role in starvation-induced autophagy. This result indicates that the ATG16L1 subunit of the LC3-lipidating enzyme is a direct and physiological target of ULK1 under starvation. We next asked if ULK1/2 or IKKα contributed to ATG16L1 phosphorylation upon infection or TNFα treatment. ULK1/2 wild-type, ULK1/2 dKO, or IKKα KO were infected with *Salmonella enterica* serovar Typhimurium (hereafter referred to as *Salmonella*) or treated with TNFα and ATG16L1 phosphorylation was examined by western blot. Surprisingly, we observed that *Salmonella* and TNFα-induced ATG16L1 phosphorylation was abolished in ULK1/2 dKO cells, but was still observed in IKKα knockout cells (Fig. 2B, EV2C). Of note, phospho-ATG16L1 signal is consistently lower under infection as only a small minority of cells are subjected to the stress of internalised bacteria (Fig. EV2D). These results clearly indicate that ULK1/2 is required for phosphorylation of ATG16L1 under starvation, inflammatory cytokine signalling and infection.

We next sought to determine the requirement for ULK1/2 and IKKα in promoting xenophagy. Xenophagic clearance of *Salmonella* is very well established and its intracellular growth is restricted by the pathway, making it an ideal model pathogen for this analysis. Wild-type or knockout cells were infected with *Salmonella* and the number of LC3B-positive *Salmonella* were quantified. LC3B is conjugated to the autophagosomal membrane and colocalises with bacteria targeted for clearance by xenophagy and can be used at early time points to monitor xenophagy induction. We found that ULK1/2-deficient cells exhibited a potent decrease in LC3B-positive bacteria, while IKKα loss did not significantly affect xenophagy (Fig. 2C, EV2E). In order to confirm the roles for ULK1/2 and IKKα in xenophagy induction and suppression of invasive bacteria we performed colony forming unit (CFU) assays in our wild-type or knockout lines. CFU assays measure bacterial viability after internalization and are inversely correlated with xenophagy rates[29]. Analysis of *Salmonella* viability 4 hours post

infection revealed that ULK1/2 dKO cells harboured a much higher number of viable internalised bacteria, indicative of an autophagy defect, when compared to wild-type and IKKα knockout cells (Fig. 2D). Surprisingly, our results indicate that ULK1/2, but not IKKα, is required for ATG16L1 phosphorylation and xenophagy induction.

ULK1 promotes cleavage of caATG16L1 through phosphorylation on S278

Multiple groups have shown that the T300A substitution in caATG16L1 renders it sensitive to caspase cleavage under stress conditions including nutrient starvation and infection[21,24,30]. Moreover, it was shown that mutation of serine 278 of ATG16L1 to alanine is involved in stress-induced caspase cleavage in the caATG16L1 background[24]. Our data indicate that ULK1 is responsible for the phosphorylation of wild-type ATG16L1 on S278 under nutrient starvation and infection. Therefore, we next sought to determine if ULK1 signalling was involved in the stress-induced destabilization of caATG16L1. HEK293A cells were transfected with either wild-type ATG16L1 or caATG16L1 co-transfected with increasing amounts of ULK1 kinase. Importantly, overexpression of ULK1 is known to result in autoactivation and induction of downstream signalling in the absence of stress, thereby allowing us to determine the isolated effect of ULK1 signalling on ATG16L1 stability independent of other stress-responsive pathways. Interestingly, we observed that ULK1 is capable of stimulating ATG16L1 cleavage and the level of cleavage is elevated in the caATG16L1 background (Fig. 3A). In order to determine if ATG16L1 cleavage was a result of ULK1-mediated phosphorylation on S278 we transfected HEK293A cells with wild-type, T300A, or S278/T300A mutants of ATG16L1 in the presence or absence of ULK1. Excitingly, we observed that single mutation of the ULK1 phosphorylation site was sufficient to reduce ULK1-driven cleavage (Fig. 3B). As expected mutation of S287, the low confidence ULK1 phosphorylation site identified by mass spectrometry, had no impact on cleavage in the T300A background (Fig. EV3A). These results indicate that caATG16L1 is preferentially cleaved through ULK1-mediated phosphorylation of S278. Conversely, we found that T300A did not have any effect on ATG16L1 phosphorylation (Fig. EV3B). Lastly, we repeated this experiment in the presence or absence of Z-VAD-FMK, a pan-caspase inhibitor, to confirm the faster migrating form of ATG16L1 was indeed a product of caspase-mediated cleavage. Treatment with a pan-caspase inhibitor resulted in a potent reduction in the levels of the faster migrating ATG16L1 band, confirming that the ULK1-driven cleavage product was a caspase cleavage product (Fig. 3C). Increasing evidence *in vitro* and *in vivo* has shown that caspase-mediated destabilization of caATG16L1 is a critical event associated with the pathobiology of this SNP[21,24]. Moreover, in unstressed conditions caATG16L1 is known to have the same stability as

wildtype[21]. To study the effect of ULK1-mediated caspase cleavage of ATG16L1 in cells we knocked out ATG16L1 using CRISPR/Cas9 (Fig. EV3C) and transfected ATG16L1(T300A) in HEK293A cells and infected cells in the presence or absence of ULK-inhibitor. Interestingly we observed *Salmonella* treatment destabilised the T300A mutant, which could be reversed with ULK-inhibitor (Fig. 3D). However, ATG16L1(WT) stability was not drastically affected by either *Salmonella* or ULK-inhibition (Fig. 3D). We also found ATG16L1(T300A) was stabilised by ULK-inhibitors under TNFα treatment (Fig. EV3D). We next sought to determine the function of S278 phosphorylation of ATG16L1 in both the wildtype and T300A background. ATG16L1 knockout cells were transfected with ATG16L1 (WT, S278A, T300A, or S278A/T300A) at similar levels and treated with *Salmonella* (Fig. EV3E). Quantification of *Salmonella* at 4 hours post infection showed that mutation of S278 phosphorylation in the wild type background resulted in an increase in *Salmonella*, indicating ULK1 phosphorylation may act to promote xenophagy in wild-type ATG16L1 (Fig. 3E, column 1 and 2). Conversely, in the T300A background S278A mutation improved *Salmonella* clearance, indicating ULK1 phosphorylation is detrimental in this background (Fig. 3E, column 3 and 4).

Collectively, our data shed light on the relationship between stress and caATG16L1 cleavage showing that: 1) ULK1-mediated phosphorylation of ATG16L1 is increased under infection and starvation, which are known to promote the cleavage of caATG16L1, 2) caATG16L1 is preferentially cleaved upon ULK1 activation, and 3) mutating the ULK1 phosphorylation site reduces ULK1-driven cleavage and improves xenophagy in the caATG16L1 background.

ULK1-mediated phosphorylation is required for ATG16L1 localization to *Salmonella* site and bacterial clearance

ULK1 kinase has a well-established role in stimulating autophagy, making it unlikely that the primary function of ULK1-induced ATG16L1 phosphorylation is to activate caspase-mediated cleavage. In order to identify the physiological role of ULK1-mediated ATG16L1 phosphorylation we performed experiments on the wild-type protein, which is not cleaved as readily after phosphorylation. The best described function of ATG16L1 is to promote the correct localization of the E3-like enzyme that lipidates LC3 to the membrane of newly forming autophagosomes. Therefore, we first sought to determine if the localization of pATG16L1 differed from that of total ATG16L1 under infection. To compare localization we infected MEF with *Salmonella* and immunostained for lipopolysaccharides (LPS), pATG16L1, and total ATG16L1. We observed pATG16L1 primarily in the infected samples, confirming the reactivity of our antibody for IF (Fig. 4A). Excitingly, we found that pATG16L1 was preferentially localised with

internalised bacteria (Fig. 4A). Analysis of total ATG16L1 staining also showed co-localization with bacteria, but also contained significantly more diffuse staining in the cytoplasm (Fig. 4A, EV4A, EV4B). This could indicate that either ULK1-mediated phosphorylation is important for ATG16L1 recruitment to bacteria, or that the phosphorylation occurs at the bacteria. We reasoned if phosphorylation of ATG16L1 affects bacterial localization then ULK1-deficient cells should exhibit an impairment in ATG16L1 recruitment to pathogen. To test this hypothesis we infected wild-type or ULK1-deficient cells and quantified the ability of total ATG16L1 to localise to internalised bacteria. Interestingly, we observed that the proportion of ATG16L1-positive bacteria in ULK1-deficient MEF was reduced by over 80% compared to the wild-type controls (Fig. 4B, EV4C, EV4D).

In order to determine the contribution of S278-phosphorylation on ATG16L1 localization to bacteria we reconstituted ATG16L1 KO cells with either wild-type ATG16L1, a truncated form of ATG16L1 that cannot bind the ULK1 complex, or the SS278A mutant and analyzed localization to intracellular bacteria. We observed that mutation of S278 or deleting the region of ATG16L1 responsible for binding the ULK1-complex resulted in a significant reduction in ATG16L1-positive bacteria (Fig. 4C, EV4E, EV4F). We then looked at colocalization between LC3B and *Salmonella* in our ATG16L mutants. We observed that the S278A mutant of ATG16L1 in the wildtype background resulted in a reduction in LC3B-positive bacteria (Fig. 4D, EV5A, EV5B). Accordingly, the S278A and Δ229-242 mutants of ATG16L1 were both defective in clearing intracellular *Salmonella* as determined by CFU assay (Fig. EV5C). In contrast S278A mutation in the T300A background increased the percentage of LC3B-positive *Salmonella* (Fig. EV5A, EV5B), which was also consistent with the decreased bacterial load observed in our CFU assay (Fig. EV3E).

To determine the role of ULK1-mediated ATG16L1 phosphorylation in starvation we starved cells reconstituted with either wild-type ATG16L1 or ATG16L1(S278A). Surprisingly, we found that S278 mutation had no effect on starvation induced autophagy flux (Fig. EV5D). These data indicate that either ULK1-mediated phosphorylation of ATG16L1 is more important under infection than starvation or additional functionally redundant signalling pathways to ATG16L1 are activated by starvation. Taken together our data indicate that ULK1-mediated phosphorylation of wild-type ATG16L1 acts to promote localization to internalised bacteria and thereby enhancing bacterial removal, while the same modification is detrimental in caATG16L1 (Fig. 4E).

Discussion

ULK1 has previously been described to phosphorylate several components of the autophagy-promoting lipid kinase complex to activate the autophagy pathway[10-12]. Here we have described that the autophagy E3-like enzyme is also regulated by ULK1 through direct phosphorylation of the ATG16L1 subunit. The discovery of a link between ULK1 and the LC3B-lipidating enzyme has raised several interesting lines of inquiry. For example, we have shown that wild-type ATG16L1 is also susceptible to ULK1-sensitive caspase-mediated cleavage, albeit at a lower level than caATG16L1. However, we currently do not know the physiological relationship between phosphorylation and caspase-mediated cleavage outside the context of the caATG16L1 allele. Potentially, caspase-mediated cleavage of ATG16L1 under stress represents a mechanism to curtail autophagy under severe or prolonged stress. Understanding the mechanistic link between apoptosis and autophagy may yield important conceptual advances.

Additionally, we have uncovered a role for ULK1-signalling in CD through regulating the stability of caATG16L1. Interestingly, the functional significance of the S278 residue in CD had already been shown[24]. However, the lack of tools to measure endogenous pATG16L1 resulted in IKKα being identified as the kinase responsible for the phosphorylation and triggering the cleavage of caATG16L1. Based on our data, as well as the previously reported link between starvation and pathogen-induced caATG16L1 dysfunction, we propose that ULK1 is the primary kinase responsible for ATG16L1 phosphorylation. However, it is quite possible that IKKα contributes to the destabilization of caATG16L1 through the previously reported activation of caspases[24].

The preferential localization of pATG16L1 to internalised bacteria is also interesting. This is because frameshifts in the gene NOD2 are strongly associated with CD-development and have also been described to affect ATG16L1 localization to internalised bacteria[17]. This may imply a common defect of ATG16L1 function in CD. Consistent with this idea CD-associated SNPs have also been described in ULK1, albeit with less strength than ATG16L1 SNPs. As we have identified a functional redundancy between ULK1 and ULK2 in the promotion of ATG16L1 phosphorylation, which may explain the weak contribution of ULK1 polymorphisms in CD-susceptibility. Lastly, transcriptional repression of IRGM has also been linked to the development of CD. Molecularly, IRGM has been shown to bind both ULK1 and ATG16L1, although they have not been shown in a complex together. Therefore, it would be of value to determine if reductions in IRGM protein would have an effect on ULK1-mediated ATG16L1 phosphorylation. Clearly, the identification of ULK1-mediated ATG16L1 phosphorylation has opened up

284 several avenues for future research, which will undoubtedly expand our understanding of xenophagy
285 and the molecular basis of autophagy defects in CD.

286

Acknowledgments

We would like to thank members of the Russell laboratory for advice and critical reading of this manuscript. We authors would like to apologise to colleagues whose significant work could not be included due to length, citation limitations, or author oversight. This work was supported by Canadian Institutes of Health Research (CIHR) Project Grants awarded to RCR (#PJT153034), the UK Dementia Research Institute (funded by MRC, Alzheimer's Research UK and the Alzheimer's Society), Wellcome Trust (Principal Research Fellowship to DCR (095317/Z/11/Z), Strategic Grant to Cambridge Institute for Medical Research (100140/Z/12/Z) and studentship to AJ, and the Roger de Spoelberch Foundation. Accademic scholarship from the government of Saudi Arabia (#5976670433) and studentship supported RA. TTL was supported by an Ontario Graduate Scholarship. Microscopy support was provided by the Cell Biology and Image Acquisition core facility, Faculty of Medicine, University of Ottawa.

Author Contributions:

TTL, RMA, and RCR wrote the manuscript. RMA and TTL were primarily responsible for data production in all figures. WT assayed endogenous pATG16L1(S278) levels under stress. AJ characterised pATG16L1(S287) function and validated the phospho-antibody. ZG performed quantification of IF images. RCR and DCR oversaw manuscript preparation, experimental planning. RCR conceived of the study.

Declaration of Interests

The authors declare no conflicts of interest.

Material and Methods

Antibodies and Reagents

Anti-IKKα (Cat#2682), HA-HRP (#Cat 2999), phospho-NF-κB S536 (Cat#3033), ATG5 (Cat#12994), NF-κB (Cat# 8242), and phospho-S6K T389 (Cat#9234) antibodies were obtained from Cell Signaling Technology. Anti-LC3B (Cat#PM036 for immunofluorescence) and ATG16L1 (Cat#PM040 for immunofluorescence) antibodies were purchased from MBL. Beta-Actin (Cat#A5441 clone AC-15) and vinculin (Cat#V9131) antibodies were obtained from Sigma. DYKDDDDK Epitope Tag (Cat#NBP1-06712 for WB) antibody was purchased from Novus Biologicals. Anti-LPS FITC (Cat#sc-52223) and GST (Cat# sc-374171) antibodies was purchased from Santa Cruz Biotechnology. Anti-S6K (Cat#ab32529), LPS (Cat#ab128709), ATG16L1 (Cat#ab187671) antibodies, and TNFα (Cat#ab9642) were obtained from Abcam. phospho-ATG16L1 serine 278 was made in collaboration with Abcam. Polyclonal sera was affinity purified by phospho peptide and recombinant ATG16L1 (non-phosphorylated) was mixed in at a 6:1 molar ratio (Rec. ATG16L1: IgG), prior to immunoblotting. Monoclonal phospho-antibody from a hybridoma generated from this rabbit was used for immunofluorescence (Abcam Cat#ab195242). Active GST-ULK1 (1-649) and GST-ULK2 (1-478) from insect cells were purchased from CQuential Solutions (Moraga, CA). Anti-His-HRP (Cat#460707) was obtained from Invitrogen. Z-VAD(OMe)-FMK (Cat#HY-16658-1MG) was purchased from MedChemExpress. Bafilomycin A1 was obtained from Tocris (Cat#133410U). ULK-inhibitor MRT68921 was obtained from Selleckchem (Cat#S7949). Digitonin (Cat#10188-874) was obtained from VWR.

Cell Culture

MEFs, HEK293A, and HCT116 were cultured in DMEM supplemented with 10% Bovine Calf Serum (VWR Life Science Seradigm). IKK wildtype and IKKα knockout MEF cells were a generous gift from Dr. Michael Karin (University of California San Diego)[31]. ULK1/2 double knockout MEF were a generous gift from Dr. Craig Thompson (Memorial Sloan Kettering)[32]. Amino acid starvation medium was prepared based on Gibco standard recipe omitting all amino acids and supplemented as above without addition of non-essential amino acids and substitution with dialyzed FBS (Invitrogen). Media was changed 1 hour before experiments.

Transfection

HEK293A cells were transfected with tagged ATG16L1 (750 ng) and tagged ULK1 (250 ng) using polyethylenimine (PEI, medistore uOttawa). HCT116 cells were transfected with the indicated tagged ATG16L1 (3-5 ug) using PEI. The samples were analyzed 48-72 hours post transfection.

Generation of knock-out cell lines using CRISPR/Cas9

ATG16L1 knock-out lines were generated in the HCT116 or HEK293A backgrounds utilizing CRISPR/Cas9 targeting exon 1. Guide RNA sequence: 5' AAACCCGCTGGAAGCGCCACATCTC 3'.

Generation of Stable Cell Lines

The knock-out clones were infected with retroviruses or lentiviruses carrying taggedATG16L1 at different amounts in order to achieve near endogenous levels of ATG16L1**.**

Site-Directed Mutagenesis

Primers used for T300A mutation are GGACAATGTGGATGCTCATCCTGGTTC (forward) and GAACCAGGATGAGCATCCACATTGTCC (reverse). Primers used for S278A mutation are GCCTTCTGGATGCTATCACTAATATC (forward) and GATATTAGTGATTGCATCCAGAAGGC (reverse). Primers used for S287A mutation are TTTGGGAGACGCGCTGTCTCTTCCT (forward) and AGGAAGAGACAGCGCGTCTCCCAAA (reverse). T300A followed by S278A or S287A mutation was performed to generate double mutations. Site-directed mutagenesis was performed based on KOD Xtreme Hot Start DNA Polymerase kit instructions purchased from Thermo Fisher. Specificity of mutagenesis was analysed by direct sequencing.

Bacterial Strains

Wild-type (SL1344) *Salmonella* was a gift from Dr. Subash Sad, (University of Ottawa). Bacteria were grown in Luria-Bertani broth (Fisher).

Bacterial Infection

Salmonella were grown in 4 mL of LB broth at 37 degrees Celsius at 250 rpm. Overnight cultures of *Salmonella* were diluted 30-fold and grown until OD_{600} reached 1.5, followed by centrifugation of 10,000 g for 2 min, and resuspension in 1 mL of PBS. Bacterial stock was then diluted 5-fold (multiplicity of infection of 900) in DMEM supplied with 10% heat-inactivated Bovine Calf Serum for infection. Cells cultured in antibiotic-free medium were infected with *Salmonella* and incubated at 37 degrees Celsius in

5% CO_2 for the indicated time. Cells were washed in PBS once before direct lysis with 1X denaturing SDS sample buffer.

Western Blot and Immunoprecipitation

Whole cell lysates were prepared by direct lysis with 1X SDS sample buffer. Samples were boiled for 10 min at 95 degrees Celsius and resolved by SDS-PAGE. Immune complexes were harvested from cells lysed in mild lysis buffer [10mM Tris pH 7.5, 10 mM EDTA, 100 mM NaCl, 50 mM NaF, 1% NP-40, supplemented simultaneously with protease and phosphatase inhibitor cocktails –EDTA (APExBIO)], followed by centrifugation at max speed for 10 minutes to remove cell debris. Protein A beads (Repligen) were washed 1X with PBS and incubated with antibodies and cell lysates for 1.5-3 hours followed by one 5-minute wash with MLB and inhibitors and 4 quick washes with MLB alone. Beads were boiled in 1X denaturing sample buffer for 10 min before resolving by SDS-PAGE.

Statistical analysis

Error bars for western blot analysis represent the standard deviation between densitometry data collected from 3 unique biological experiments. Statistical significance was determined using paired Student's two-tailed T-test for two data sets.

Immunofluorescence

Cells were plated on IBDI-treated coverslips overnight. After treatments, cells were fixed by 4% paraformaldehyde in PBS for 15 min and subsequently permeabilised with 50 µg/mL digitonin in PBS for 10 min at room temperature. Cells were blocked in blocking buffer (1% BSA and 2% serum in PBS) for 30 min, followed by incubation with primary antibodies in the same buffer for one hour at room temperature. Samples were then washed 2X in PBS and 1X in blocking buffer before incubation with secondary antibodies one hour at room temperature. Slides were washed 3X in PBS, stained with DAPI, and mounted. Images were captured with inverted epifluorescent Zeiss AxioObserver.Z1. In the case of outside/inside bacterial staining, before permeabilization, the cells were incubated with anti-LPS antibody and corresponding secondary antibody in blocking buffer, accompanied by 3X PBS washes in between.

Quantification of Immunofluorescence

An automated protocol built in the Image J software was used to analyse epifluorescent microscopy images to avoid bias. The same protocol was applied to each field of view and across samples. An average of 8 unique fields of view from representative experiments were selected for quantification.

***in vitro* ULK1 Kinase Assay**

HEK293A transiently expressing tagged ATG16L1 were immunoprecipitated. Pulldown proteins were washed 3X with MLB and 1X with MOPS buffer and were used as substrates for ULK1 kinase assay. ULK1 proteins were immunoprecipitated and extensively washed with MLB (once) and RIPA buffer (50 mM Tris at pH 7.5, 150 mM NaCl, 50 mM NaF, 1 mM EDTA, 1 mM EGTA, 1% SDS, 1% Triton X-100 and 0.5% deoxycholate) once, followed by washing with MLB buffer once followed by equilibration with ULK1 assay buffer (kinase base buffer supplemented with 0.05 mM DTT, 10 μM cold ATP, and 0.4 μCil ^{32}P-ATP per reaction). Reactions were shaken at 250 rpm at 37 degrees Celsius for 30 min and stopped by direct addition of 4X sample buffer followed by 10 min boiling at 95 degrees Celsius and resolution by SDS-PAGE. The analysis of kinase reactions necessitated the separation of the kinase and substrate. *In vitro* kinase reactions were analyzed by autoradiograms.

Colony Forming Unit (CFU) Assay

Cells were infected with *Salmonella* (MOI of 180) for 1 hour. The infected cells were washed 2X and incubated with media containing 100 μg/mL Gentamicin for 0.5 hour, followed by 4-hour incubation with media containing 50 μg/mL Gentamicin. The samples were rinsed 3X with PBS and lysed with CFU buffer (0.1% Triton X-100 and 0.01% SDS in PBS). The harvested lysates were serially diluted (1:100, 1:300, and 1:1000) and plated onto LB agar plates containing Streptomycin. The plates were incubated at 37 degrees Celsius for 16-18 hours and the colonies were counted to determine the number of CFU.

Figure Legends

Figure1

ATG16L1 is phosphorylated by ULK1

(A) in *vitro* kinase assays were performed using purified recombinant kinases (ULK1 and ULK2) and substrate (ATG16L1) in the presence of radiolabelled ATP. ULK and ATG16L1 inputs were examined by western blot (WB) and substrate phosphorylation was analyzed by autoradiography (AR).

(B) Full-length or truncated versions of ATG16L1 were subjected to an *in vitro* ULK1 kinase assay. ULK1 and ATG16L1 inputs were examined by western blot and target phosphorylation by autoradiography.

(C) ATG16L1 was phosphorylated in an *in vitro* ULK1 kinase reaction and analysed by mass spectrometry. Phosphorylation of S278 and S287 in human (S278 marked in green, S287 marked in grey) was identified with high and low confidence, respectively. Conservation of amino acids 254-294 are shown using the Shapely colour scheme. Mass spectrometry was performed on a single experiment.

(D) Full-length or mutated HA-ATG16L1 was purified from mammalian cells and subjected to an *in vitro* ULK1 kinase assay. Inputs were analysed by WB and target phosphorylation by AR.

(E) HEK293A cells were transfected with wild-type or phospho-dead ATG16L1 in the presence of wild-type or kinase-dead ULK1. Phosphorylation of ATG16L1 (S278 or S287) and inputs were examined by WB.

Data information: Unless otherwise indicated experiments were performed three times.

Figure 2

ULK1/2 is required for phosphorylation of ATG16L1 and xenophagy induction

(A) Wild-type, ULK1/2 double knockout (dKO), or IKKα KO mouse embryonic fibroblasts (MEFs) were incubated with either complete medium, amino acid-deficient DMEM, or HBSS for 1 hour. Samples were immunoblotted using the indicated antibodies.

(B) Wild-type, ULK1/2 dKO, or IKKα KO MEFs were infected with log phase *Salmonella* for 2 hours; bacteria-containing media was then removed and cells were incubated with gentamycin (50 μg/mL)-containing DMEM for 2 hours. Samples were immunoblotted using the indicated antibodies.

(C) Wild-type, ULK1/2 dKO, or IKKα KO MEFs cells were infected with *Salmonella* for 1 hours. Autophagic capture of *Salmonella* was analyzed by immunostaining for LPS and LC3B. Representative images are shown (scale bars, 10 μm and 3 μm). Quantification was generated from 8 fields of view from a representative experiment. The experiments were repeated twice.

(D) Wild-type, ULK1/2 dKO and IKKα KO MEFs were infected with *Salmonella* for 1 hour. Xenophagy rates were examined through Colony Forming Unit (CFU) assays. Quantification of infection rates by immunofluorescence is demonstrated in the right panel.

Data information: Unless otherwise indicated experiments were performed three times. Data are represented as mean ± standard deviation and p values were determined by Student's T-Test.

Figure 3

ULK1 promotes cleavage of T300A ATG16L1 through phosphorylation on S278

(A) HEK293A cells were transfected with either flag-tagged WT ATG16L1 or T300A ATG16L1. ULK1 was co-transfected in increasing amounts where indicated. Cleavage of ATG16L1 was analyzed by WB of whole cell lysates. Levels of ATG16L1 cleavage were quantified from 3 biological repeats (right panel).

(B) HEK293A cells were transfected with either tagged wild-type, T300A, or S278/T300A ATG16L1 in the presence or absence of ULK1. Cleavage of ATG16L1 was analyzed by WB. Levels of ATG16L1 cleavage were measured from 3 biological repeats (right panel).

(C) HEK293A cells were transfected with the indicated plasmids in the presence or absence of a pan-caspase inhibitor Z-VAD-FMK (15 μM) for 4 hours. Cleavage of ATG16L1 was analyzed by WB of 3 biological repeats.

(D) Wild-type or T300A-expressing HEK293A were treated with *Salmonella* in the presence or absence of ULK1/2 inhibitor (16 μM) for the indicated time points. Expression of ATG16L1 was analysed by WB. The experiments were performed twice.

(E) ATG16L1 knock-out HEK293A cells transfected with the indicated HA GST ATG16L1 plasmids were infected with *Salmonella* for 1 hour. Xenophagy rates were examined through CFU assays. Quantification of infection rates by immunofluorescence is demonstrated in the right panel.

Data information: Unless otherwise indicated experiments were performed three times. Data are represented as mean ± standard deviation and p values were determined by Student's T-Test.

Figure 4

ULK1-mediated phosphorylation is required for ATG16L1 localization to *Salmonella* site and bacterial clearance

(A) Wild-type MEF cells were infected with *Salmonella* for 25 minutes. Phospho-ATG16L1, total ATG16L1, and LPS were stained and analysed by immunofluorescence. Representative immunofluorescent images are shown (scale bars, 10 μm and 1 μm).

(B) Wild-type and ULK1/2 dKO were infected with *Salmonella* for 25 minutes. Immunofluorescence was performed using antibodies against LPS and ATG16L1. Representative immunofluorescent images are shown on the left panel (scale bars, 10 μm and 2 μm). Quantification of ATG16L1-positive bacteria from 7 fields of view from a representative experiment is shown in the right panel.

(C) ATG16L1 knock-out HCT116 transfected with the indicated GST HA ATG16L1 were infected with *Salmonella* for 1 hour. Bacteria were stained using anti-LPS antibodies to analyze localization in addition to ATG16L1. Representative immunofluorescent images of ATG16L1 and LPS are shown (scale bars, 5μm and 1 μm). Quantification of ATG16L1 localizing to bacteria from 7 fields of view from a representative experiment is shown in the lower panel.

(D) ATG16L1 knock-out HCT116 transfected with the indicated GST HA ATG16L1 were infected with *Salmonella* for 1 hour. Bacteria were stained using anti-LPS antibodies to analyze localization in addition to the autophagy marker LC3B. Representative immunofluorescent images of LC3B and LPS are shown

493 (scale bars, 5µm and 1 µm). Quantification of bacteria undergoing autophagic clearance from 7 fields of
494 view from a representative experiment is shown in the lower panel.

495 (E) A diagram demonstrating our working model for the role of ULK1-mediated phosphorylation at S278
496 in wild-type and T300A ATG16L1 background.

497 Data information: Unless otherwise indicated experiments were performed twice. Data are represented
498 as mean and p values were determined by Student's T-Test.

499

Expanded View Figure Legends

Figure EV1

ATG16L1 is a target of ULK1 kinase

(A) Mass spectrometry data for ULK1-mediated ATG16L1 phosphorylation.

(B) ATG16L1 knock-out HEK293A were transfected with either flag-tagged wild-type or S287A ATG16L1. Phosphorylation of ATG16L1 at S287 was determined by WB.

(C) Wild-type ATG16L1 substrate and ULK1 were incubated with or without lamda phosphatase. Phospho-specificity of ATG16L1(S287) antibody was determined by immunoblot for total- and phospho-ATG16L1.

Figure EV2

ULK1 is required for phosphorylation of ATG16L1 and xenophagy induction

(A) Full scan for WB data for phospho-ATG16L1(S278) shown in Fig. 2A.

(B) ATG16L1 knock-out HEK293A transfected with the indicated GST HA ATG16L1 plasmids were immunoprecipitated for HA. WB was used to examine the binding of ATG5/ATG12 to ATG16L1.

(C) Wild-type, ULK1/2 dKO, or IKKα KO MEFs were treated with either amino acid-free media or the indicated amounts of TNFα for 3 hours. Samples were immunoblotted using the indicated antibodies. Levels of ATG16L1 phosphorylation were quantified from three biological replicates. Data are represented as mean ± standard deviation and p values were determined by Student's T-Test.

(D) Wild-type, ULK1/2 dKO and IKKα KO MEFs were infected with *Salmonella* for 1 hour. Quantification of infected cells were examined through immunofluorescence of two biological repeats. Data are represented as mean ± standard deviation from 7 unique fields of view and p values were determined by Student's T-Test.

(E) Larger field of view for images shown in Fig. 2C. Extracellular bacteria staining observable in white. MEF cells were infected with *Salmonella* for 1 hour in the presence of Bafilomycin A1. Endogenous LC3B (red) puncta was visualised (scale bars, 20 μm and 10 μm) by immunofluorescence. Dashed boxes represent the cells selected for enlarged display in Fig. 2C.

(F) Quantification of LC3B-positive bacteria of Fig. 2C biological replicate. Wild-type, ULK1/2 dKO, or IKKα KO MEFs cells were infected with *Salmonella* for 1 hours. Autophagic capture of *Salmonella* was analyzed by immunostaining for LPS and LC3B. Data are represented as mean and p values were determined by Student's T-Test.

Figure EV3

ULK1 promotes cleavage of caATG16L1 through phosphorylation on S278

(A) ATG16L1 knock-out HEK293A were transfected with the indicated GST HA ATG16L1 plasmids in the presence or absence of Z-VAD-FMK (15 μM) for 4 hours. Cleavage of ATG16L1 was analyzed by WB of

two biological replicates. Data are represented as mean values and p values were determined by Student's T-Test.

(B) ATG16L1 knock-out HEK293A were transfected with the indicated GST HA ATG16L1 plasmids in the presence or absence of Z-VAD-FMK (15 μM) for 4 hours. Phosphorylation of ATG16l1 was analyzed by WB.

(C) ATG16L1 knock-out cells were validated by direct sequencing.

(D) ATG16L1 knock-out HCT116 transfected with the tagged T300A ATG16L1 plasmids were treated with TNFα (20 ng/mL) in the presence or absence of ULK1/2 inhibitor for 4 hours. ATG16L1 levels were examined by WB.

(E) Inputs for CFU assays in Fig. 3E. ATG16L1 knock-out HEK293A transfected with tagged ATG16L1 as indicated were lysed and examined by WB.

Figure EV4

ULK1-mediated phosphorylation is required for ATG16L1 localization to *Salmonella* site

(A) Larger field of view for images shown in Fig. 4A. Bacteria staining observable in white. MEF cells were infected with *Salmonella* for 25 minutes. Phospho-ATG16L1 (red) and total ATG16L1 (green) were visualised (scale bars, 20 μm and 10 μm) by immunofluorescence. Dashed boxes represent the cells selected for enlarged display in Fig. 4A.

(B) Quantification of ATG16L1 localization to the bacteria of Fig. 4A biological replicate. Wild-type MEF cells were infected with *Salmonella* for 25 minutes. Phospho-ATG16L1, total ATG16L1, and LPS were stained and analysed by immunofluorescence. Data are represented as mean and p values were determined by Student's T-Test.

(C) Larger field of view for images shown in Fig. 4B. Extracellular bacteria staining observable in white. MEF cells were infected with *Salmonella* for 25 minutes. Endogenous ATG16L1 (red) puncta was visualised (scale bars, 30 μm and 10 μm) by immunofluorescence. Dashed boxes represent the cells selected for enlarged display in Fig. 4B.

(D) Quantification of ATG16L1 puncta of Fig. 4B biological replicate. Wild-type and ULK1/2 dKO were infected with *Salmonella* for 25 minutes. Immunofluorescence was performed using antibodies against LPS and ATG16L1. Data are represented as mean and p values were determined by Student's T-Test.

(E) Larger field of view for images shown in Fig. 4C and extra data from the same experiment were also included. ATG16L1 knock-out HCT116 transfected with the indicated GST HA ATG16L1 were infected with *Salmonella* for 1 hour. ATG16L1 (red) puncta was analysed by immunofluorescence (scale bars, 10 μm, 5 μm, and 1 μm). The experiments were repeated twice. Data are represented as mean ± standard deviation from 7 unique fields of view and p values were determined by Student's T-Test.

(F) Quantification of ATG16L1-positive bacteria of Fig. 4C biological replicate. ATG16L1 knock-out HCT116 transfected with the indicated GST HA ATG16L1 were infected with *Salmonella* for 1 hour. Bacteria were stained using anti-LPS antibodies to analyze localization in addition to ATG16L1. Data are represented as mean and p values were determined by Student's T-Test.

Figure EV5

ULK1-mediated phosphorylation is required for xenophagy and bacterial clearance

(A) Larger field of view for images shown in Fig. 4D and extra data from the same experiment were also included. ATG16L1 knock-out HCT116 transfected with the indicated GST HA ATG16L1 were infected with *Salmonella* for 1 hour. LC3B (red) puncta was analysed by immunofluorescence (scale bars, 10 µm, 5 µm, and 1 µm). The experiments were repeated twice. Data are represented as mean ± standard deviation from 7 unique fields of view and p values were determined by Student's T-Test.

(B) Quantification of LC3B-positive bacteria of Fig. 4D biological replicate. ATG16L1 knock-out HCT116 transfected with the indicated GST HA ATG16L1 were infected with *Salmonella* for 1 hour. Bacteria were stained using anti-LPS antibodies to analyze localization in addition to the autophagy marker LC3B. Data are represented as mean and p values were determined by Student's T-Test.

(C) ATG16L1 knock-out HEK293A cells transfected with the indicated HA GST ATG16L1 plasmids were infected with *Salmonella* for 1 hour. Xenophagy rates were examined through CFU assays. Quantification of infection rates by immunofluorescence is demonstrated in the middle panel. Expression of ATG16L1 was examined by WB (bottom panel). The experiments were repeated three times. Data are represented as mean ± standard deviation and p values were determined by Student's T-Test.

(D) ATG16L1 KO HCT116 with or without the indicated reconstituted OLLAS ATG16L1 were incubated with HBSS media in the presence of bafilomycin A1 for 1 hour. LC3B flux was analysed by WB. The experiments were repeated three times. Data are represented as mean ± standard deviation and p values were determined by Student's T-Test.

References

1. Parzych, K.R. & Klionsky, D.J. An overview of autophagy: morphology, mechanism, and regulation. *Antioxid Redox Signal* **20**, 460-473 (2014).
2. Kim, J., Kundu, M., Viollet, B. & Guan, K.L. AMPK and mTOR regulate autophagy through direct phosphorylation of Ulk1. *Nat Cell Biol* **13**, 132-141 (2011).
3. Yuan, H.X., Russell, R.C. & Guan, K.L. Regulation of PIK3C3/VPS34 complexes by MTOR in nutrient stress-induced autophagy. *Autophagy* **9**, 1983-1995 (2013).
4. Hosokawa, N*., et al.* Nutrient-dependent mTORC1 association with the ULK1-Atg13-FIP200 complex required for autophagy. *Mol Biol Cell* **20**, 1981-1991 (2009).
5. Ganley, I.G*., et al.* ULK1.ATG13.FIP200 complex mediates mTOR signaling and is essential for autophagy. *J Biol Chem* **284**, 12297-12305 (2009).
6. Underwood, B.R*., et al.* Antioxidants can inhibit basal autophagy and enhance neurodegeneration in models of polyglutamine disease. *Hum Mol Genet* **19**, 3413-3429 (2010).
7. Russell, R.C., Yuan, H.X. & Guan, K.L. Autophagy regulation by nutrient signaling. *Cell Res* **24**, 42-57 (2014).
8. Gomes, L.C. & Dikic, I. Autophagy in antimicrobial immunity. *Mol Cell* **54**, 224-233 (2014).
9. McAlpine, F., Williamson, L.E., Tooze, S.A. & Chan, E.Y. Regulation of nutrient-sensitive autophagy by uncoordinated 51-like kinases 1 and 2. *Autophagy* **9**, 361-373 (2013).
10. Russell, R.C*., et al.* ULK1 induces autophagy by phosphorylating Beclin-1 and activating VPS34 lipid kinase. *Nat Cell Biol* **15**, 741-750 (2013).
11. Park, J.M*., et al.* The ULK1 complex mediates MTORC1 signaling to the autophagy initiation machinery via binding and phosphorylating ATG14. *Autophagy* **12**, 547-564 (2016).
12. Di Bartolomeo, S*., et al.* The dynamic interaction of AMBRA1 with the dynein motor complex regulates mammalian autophagy. *J Cell Biol* **191**, 155-168 (2010).
13. Fan, W., Nassiri, A. & Zhong, Q. Autophagosome targeting and membrane curvature sensing by Barkor/Atg14(L). *Proc Natl Acad Sci U S A* **108**, 7769-7774 (2011).
14. Fujita, N*., et al.* The Atg16L complex specifies the site of LC3 lipidation for membrane biogenesis in autophagy. *Mol Biol Cell* **19**, 2092-2100 (2008).
15. Randow, F. & Youle, R.J. Self and nonself: how autophagy targets mitochondria and bacteria. *Cell Host Microbe* **15**, 403-411 (2014).
16. Chauhan, S., Mandell, M.A. & Deretic, V. IRGM governs the core autophagy machinery to conduct antimicrobial defense. *Mol Cell* **58**, 507-521 (2015).
17. Travassos, L.H*., et al.* Nod1 and Nod2 direct autophagy by recruiting ATG16L1 to the plasma membrane at the site of bacterial entry. *Nat Immunol* **11**, 55-62 (2010).
18. Parkes, M. Evidence from genetics for a role of autophagy and innate immunity in IBD pathogenesis. *Dig Dis* **30**, 330-333 (2012).
19. Massey, D.C. & Parkes, M. Genome-wide association scanning highlights two autophagy genes, ATG16L1 and IRGM, as being significantly associated with Crohn's disease. *Autophagy* **3**, 649-651 (2007).
20. Sadaghian Sadabad, M*., et al.* The ATG16L1-T300A allele impairs clearance of pathosymbionts in the inflamed ileal mucosa of Crohn's disease patients. *Gut* **64**, 1546-1552 (2015).
21. Murthy, A*., et al.* A Crohn's disease variant in Atg16l1 enhances its degradation by caspase 3. *Nature* **506**, 456-462 (2014).
22. Sorbara, M.T*., et al.* The protein ATG16L1 suppresses inflammatory cytokines induced by the intracellular sensors Nod1 and Nod2 in an autophagy-independent manner. *Immunity* **39**, 858-873 (2013).

642 23. Homer, C.R., Richmond, A.L., Rebert, N.A., Achkar, J.P. & McDonald, C. ATG16L1 and NOD2
643 interact in an autophagy-dependent antibacterial pathway implicated in Crohn's disease
644 pathogenesis. *Gastroenterology* **139**, 1630-1641, 1641 e1631-1632 (2010).
645 24. Diamanti, M.A*., et al.* IKKalpha controls ATG16L1 degradation to prevent ER stress during
646 inflammation. *J Exp Med* **214**, 423-437 (2017).
647 25. Gao, P*., et al.* The Inflammatory Bowel Disease-Associated Autophagy Gene Atg16L1T300A Acts
648 as a Dominant Negative Variant in Mice. *J Immunol* **198**, 2457-2467 (2017).
649 26. Boada-Romero, E*., et al.* The T300A Crohn's disease risk polymorphism impairs function of the
650 WD40 domain of ATG16L1. *Nat Commun* **7**, 11821 (2016).
651 27. Gammoh, N., Florey, O., Overholtzer, M. & Jiang, X. Interaction between FIP200 and ATG16L1
652 distinguishes ULK1 complex-dependent and -independent autophagy. *Nat Struct Mol Biol* (2012).
653 28. Nishimura, T*., et al.* FIP200 regulates targeting of Atg16L1 to the isolation membrane. *EMBO Rep*
654 **14**, 284-291 (2013).
655 29. Alonso, S., Pethe, K., Russell, D.G. & Purdy, G.E. Lysosomal killing of Mycobacterium mediated by
656 ubiquitin-derived peptides is enhanced by autophagy. *Proc Natl Acad Sci U S A* **104**, 6031-6036
657 (2007).
658 30. Santeford, A*., et al.* Impaired autophagy in macrophages promotes inflammatory eye disease.
659 *Autophagy* **12**, 1876-1885 (2016).
660 31. Hu, Y*., et al.* Abnormal morphogenesis but intact IKK activation in mice lacking the IKKalpha
661 subunit of IkappaB kinase. *Science* **284**, 316-320 (1999).
662 32. Cheong, H., Lindsten, T., Wu, J., Lu, C. & Thompson, C.B. Ammonia-induced autophagy is
663 independent of ULK1/ULK2 kinases. *Proc Natl Acad Sci U S A* **108**, 11121-11126 (2011).

664

1.

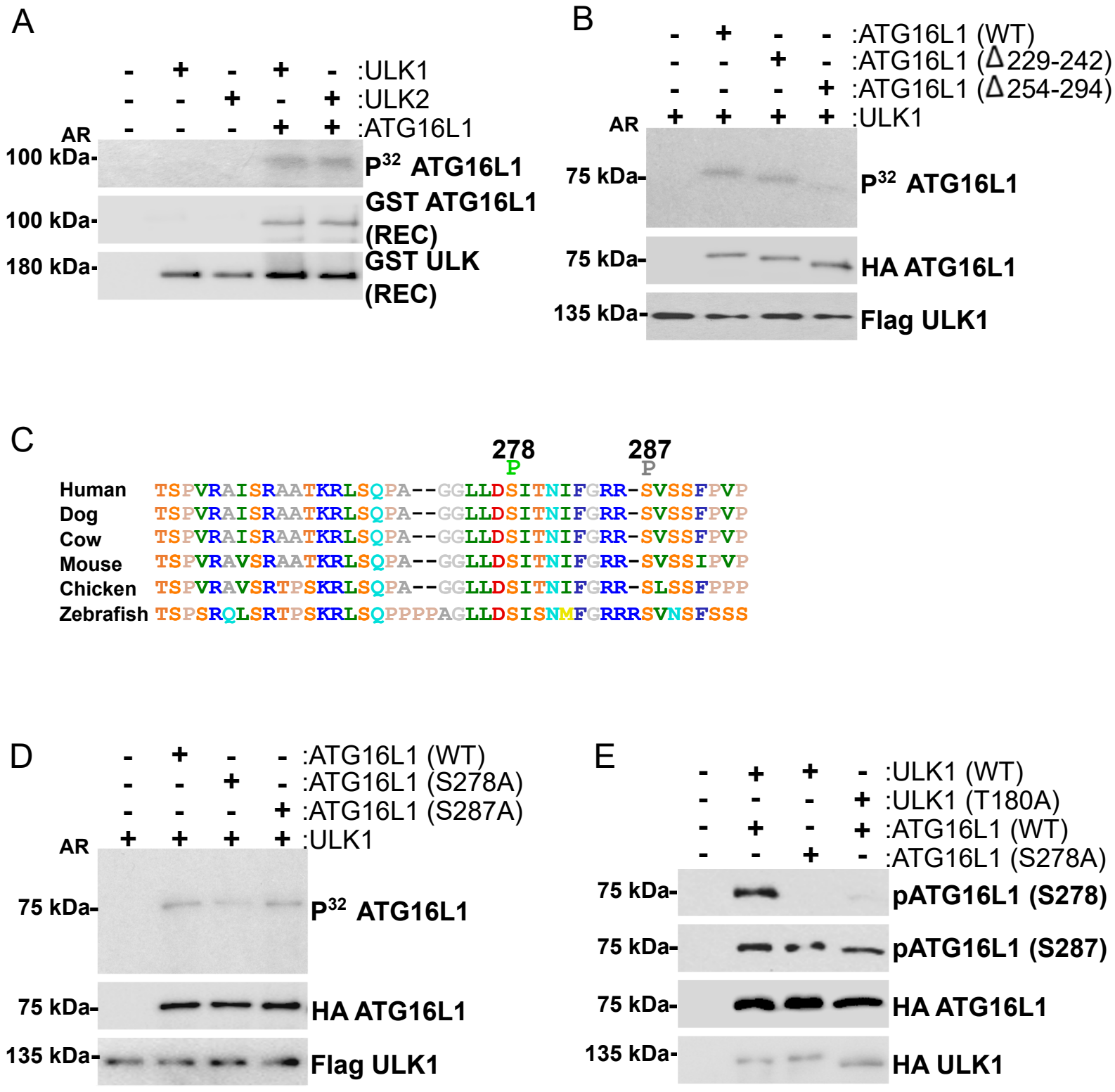
A
- + - + - :ULK1
- - + - + :ULK2
AR - - - + + :ATG16L1
100 kDa-
P32 ATG16L1
GST ATG16L1 (REC)
100 kDa-
180 kDa-
GST ULK (REC)
B
- + - - :ATG16L1 (WT)
- - + - :ATG16L1 (Δ229-242)
- - - + :ATG16L1 (Δ254-294)
AR + + + + :ULK1
75 kDa-
P32 ATG16L1
75 kDa-
HA ATG16L1
135 kDa-
Flag ULK1
C
278 P
287 P
Human TSPVRAISRAATKRLSQPA--GGLLDSITNIFGRR-SVSSFPVP
Dog TSPVRAISRAATKRLSQPA--GGLLDSITNIFGRR-SVSSFPVP
Cow TSPVRAISRAATKRLSQPA--GGLLDSITNIFGRR-SVSSFPVP
Mouse TSPVRAVSRAATKRLSQPA--GGLLDSITNIFGRR-SVSSIPVP
Chicken TSPVRAVSRTPSKRLSQPA--GGLLDSITNIFGRR-SLSSFPPP
Zebrafish TSPSRQLSRTPSKRLSQPPPPAGLLDSISNMFGRRRSVNSFSSS
D
- + - - :ATG16L1 (WT)
- - + - :ATG16L1 (S278A)
- - - + :ATG16L1 (S287A)
AR + + + + :ULK1
75 kDa-
P32 ATG16L1
75 kDa-
HA ATG16L1
135 kDa-
Flag ULK1
E
- + + - :ULK1 (WT)
- - - + :ULK1 (T180A)
- + - + :ATG16L1 (WT)
- - + - :ATG16L1 (S278A)
75 kDa-
pATG16L1 (S278)
75 kDa-
pATG16L1 (S287)
75 kDa-
HA ATG16L1
135 kDa-
HA ULK1

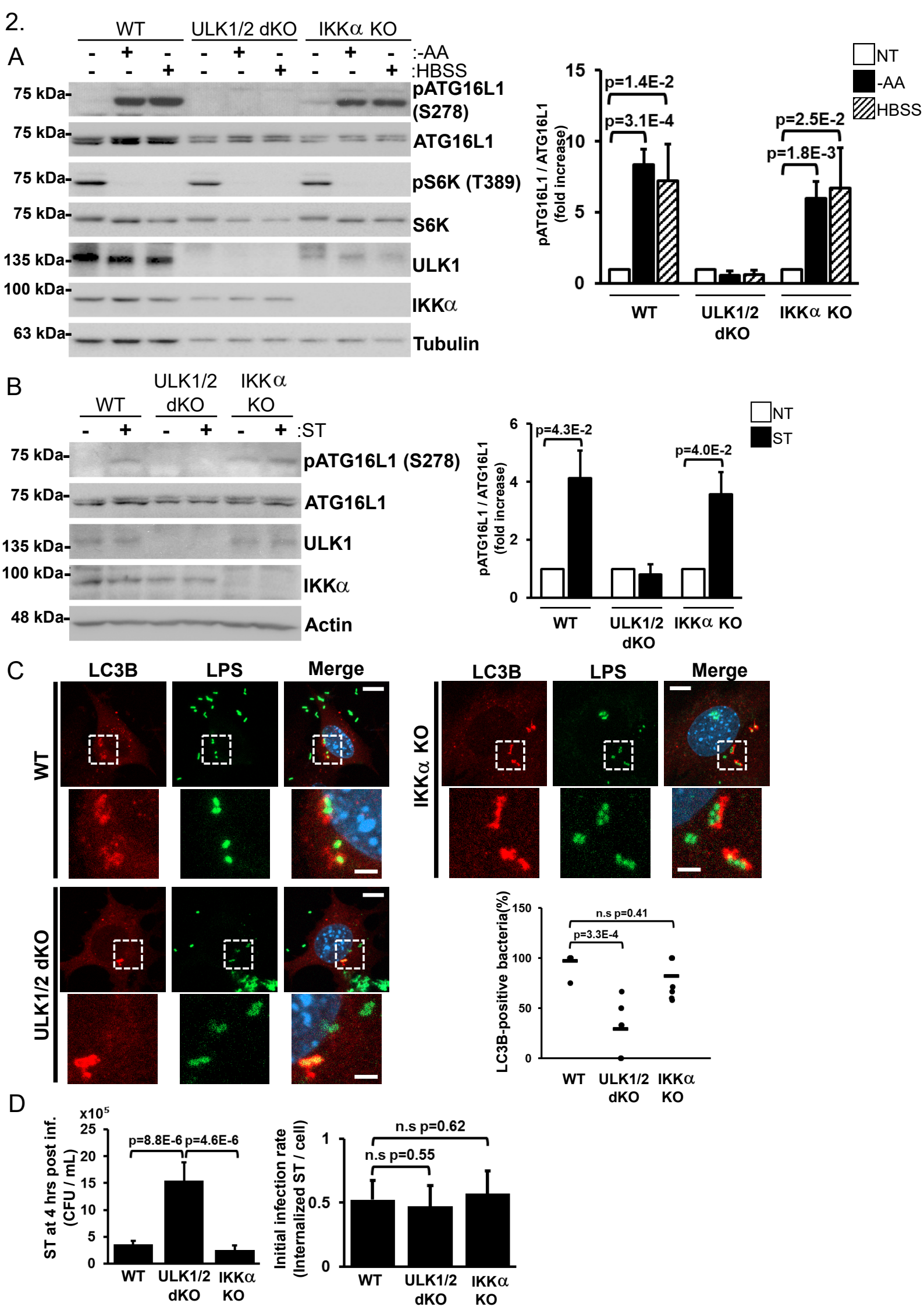
2.
A
WT
ULK1/2 dKO
IKKα KO
:-AA
:HBSS
75 kDa
pATG16L1 (S278)
ATG16L1
pS6K (T389)
S6K
135 kDa
ULK1
100 kDa
IKKα
63 kDa
Tubulin
NT
-AA
HBSS
pATG16L1 / ATG16L1 (fold increase)
p=1.4E-2
p=3.1E-4
p=2.5E-2
p=1.8E-3
B
ST
48 kDa
Actin
p=4.3E-2
p=4.0E-2
C
LC3B
LPS
Merge
WT
IKKα KO
ULK1/2 dKO
LC3B-positive bacteria(%)
n.s p=0.41
p=3.3E-4
D
ST at 4 hrs post inf. (CFU / mL)
x10^5
p=8.8E-6
p=4.6E-6
Initial infection rate (Internalized ST / cell)
n.s p=0.62
n.s p=0.55

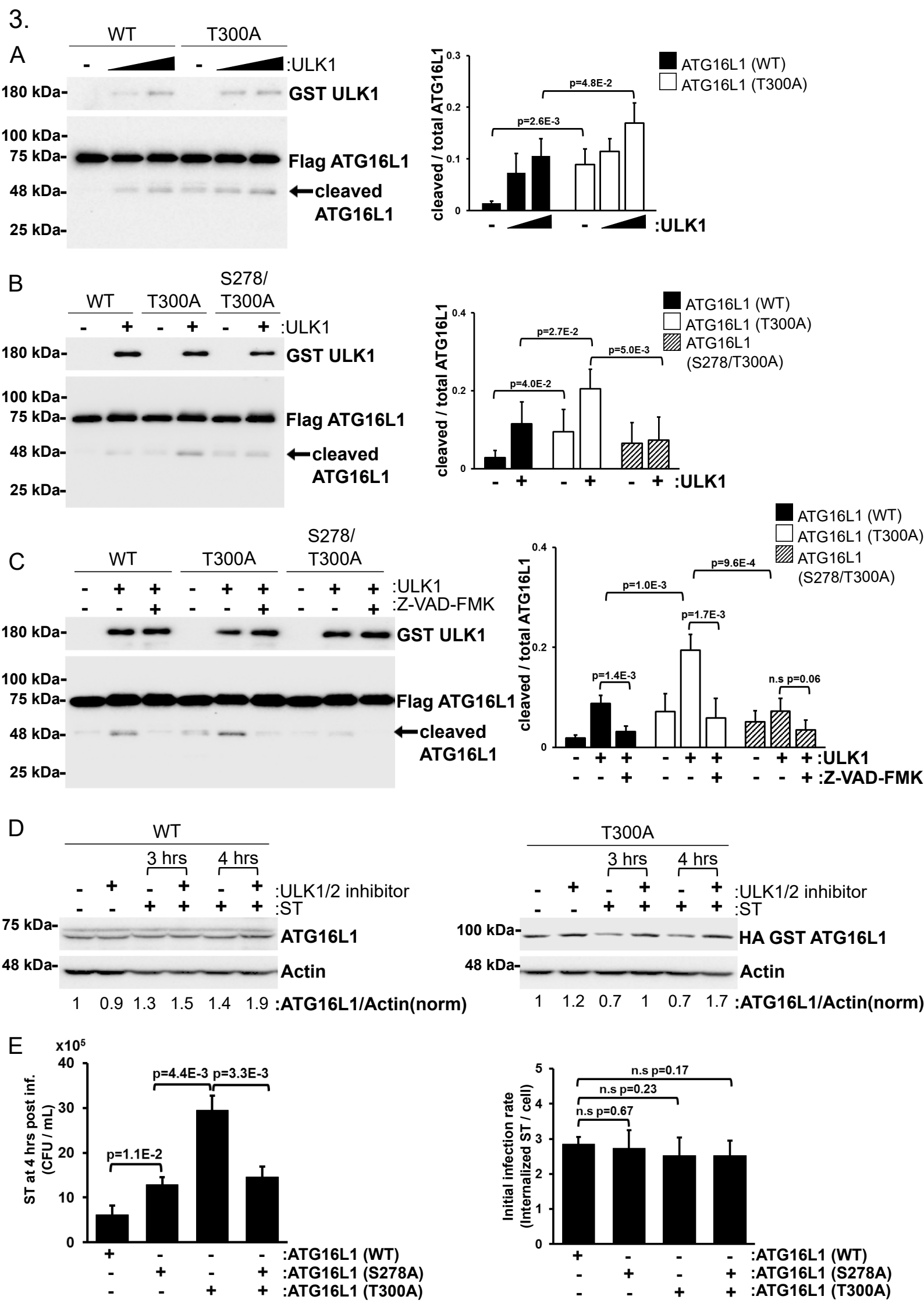
3.
A
WT
T300A
:ULK1
180 kDa-
GST ULK1
100 kDa-
75 kDa-
Flag ATG16L1
48 kDa-
cleaved ATG16L1
25 kDa-
cleaved / total ATG16L1
ATG16L1 (WT)
ATG16L1 (T300A)
p=4.8E-2
p=2.6E-3
B
S278/ T300A
ATG16L1 (S278/T300A)
p=2.7E-2
p=5.0E-3
p=4.0E-2
C
:Z-VAD-FMK
p=9.6E-4
p=1.0E-3
p=1.7E-3
p=1.4E-3
n.s p=0.06
D
3 hrs
4 hrs
:ULK1/2 inhibitor
:ST
75 kDa-
ATG16L1
48 kDa-
Actin
1 0.9 1.3 1.5 1.4 1.9 :ATG16L1/Actin(norm)
100 kDa-
HA GST ATG16L1
1 1.2 0.7 1 0.7 1.7 :ATG16L1/Actin(norm)
E
x10^5
ST at 4 hrs post inf. (CFU / mL)
p=1.1E-2
p=4.4E-3
p=3.3E-3
:ATG16L1 (WT)
:ATG16L1 (S278A)
:ATG16L1 (T300A)
Initial infection rate (Internalized ST / cell)
n.s p=0.17
n.s p=0.23
n.s p=0.67

4.

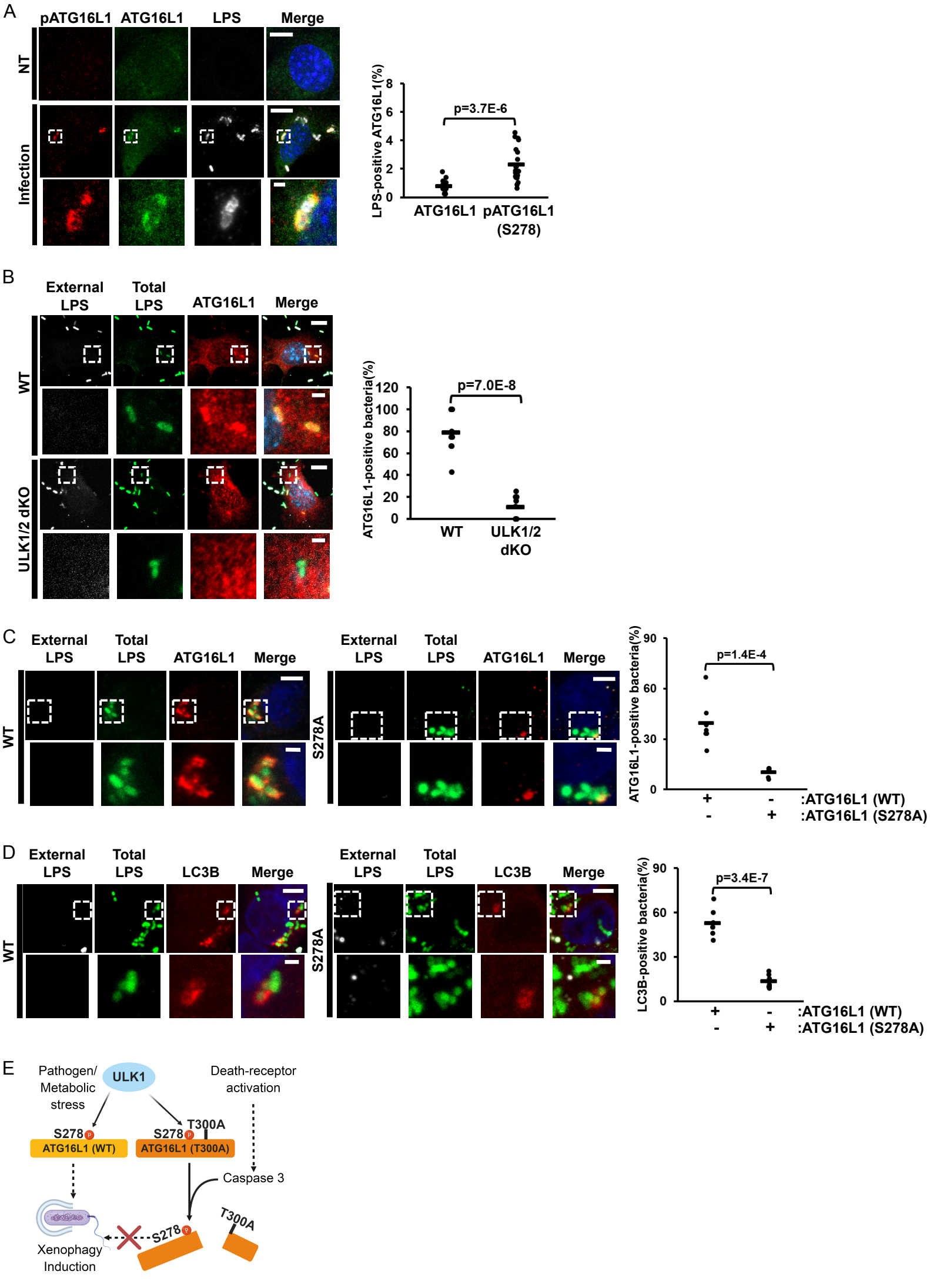
A
pATG16L1
ATG16L1
LPS
Merge
NT
Infection
LPS-positive ATG16L1(%)
p=3.7E-6
ATG16L1
pATG16L1 (S278)
B
External LPS
Total LPS
ATG16L1
Merge
WT
ULK1/2 dKO
ATG16L1-positive bacteria(%)
p=7.0E-8
WT
ULK1/2 dKO
C
External LPS
Total LPS
ATG16L1
Merge
WT
S278A
ATG16L1-positive bacteria(%)
p=1.4E-4
:ATG16L1 (WT)
:ATG16L1 (S278A)
D
External LPS
Total LPS
LC3B
Merge
WT
S278A
LC3B-positive bacteria(%)
p=3.4E-7
:ATG16L1 (WT)
:ATG16L1 (S278A)
E
Pathogen/ Metabolic stress
ULK1
Death-receptor activation
S278
ATG16L1 (WT)
T300A
ATG16L1 (T300A)
Caspase 3
Xenophagy Induction

EV1.

A

pS278

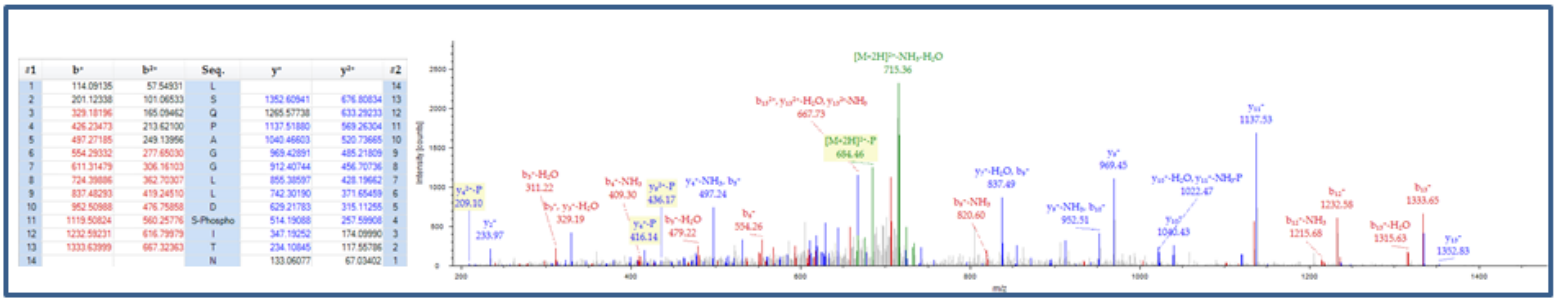

pS287

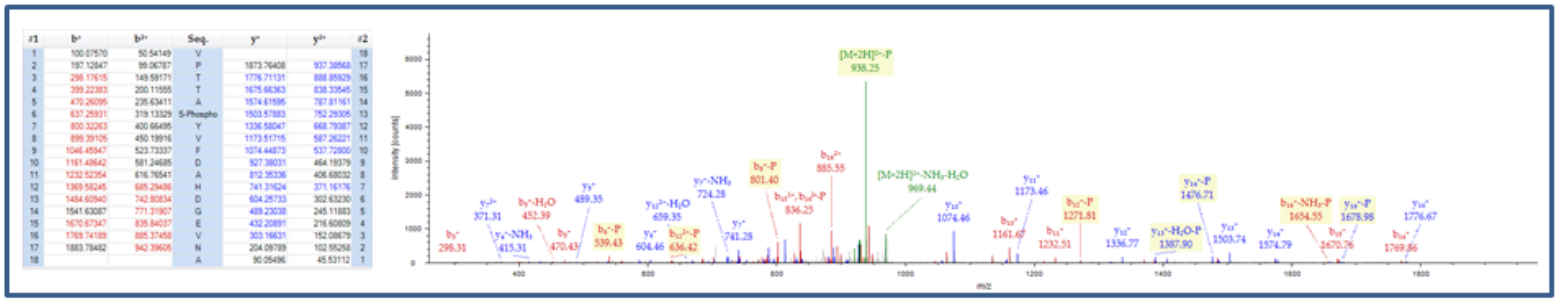

B

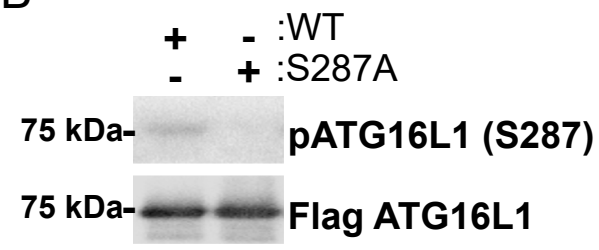

C

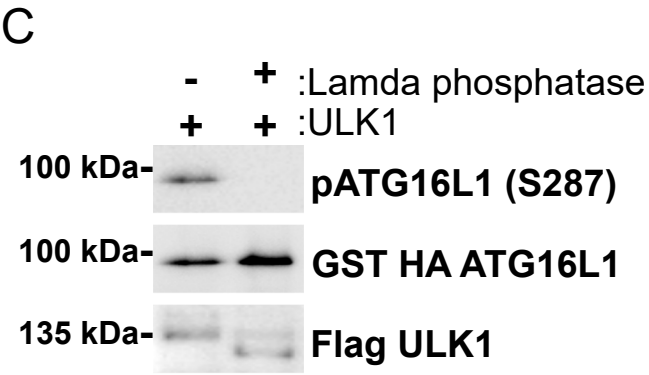

EV2.

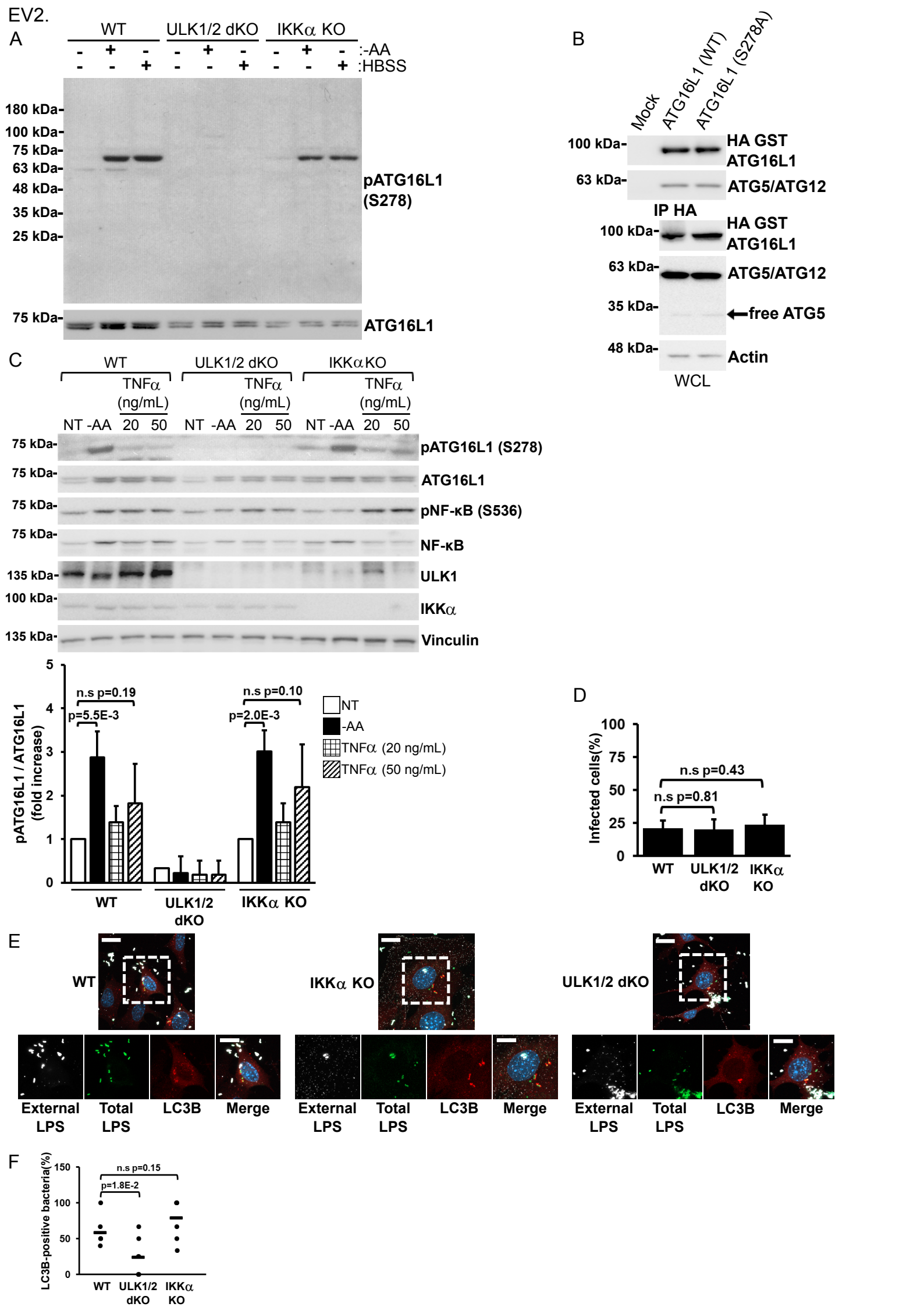
A
WT
ULK1/2 dKO
IKKα KO
-AA
HBSS
180 kDa
100 kDa
75 kDa
63 kDa
48 kDa
35 kDa
25 kDa
pATG16L1 (S278)
75 kDa
ATG16L1
B
Mock
ATG16L1 (WT)
ATG16L1 (S278A)
100 kDa
HA GST ATG16L1
63 kDa
ATG5/ATG12
IP HA
100 kDa
HA GST ATG16L1
63 kDa
ATG5/ATG12
35 kDa
free ATG5
48 kDa
Actin
WCL
C
WT
ULK1/2 dKO
IKKαKO
TNFα (ng/mL)
NT -AA 20 50
75 kDa
pATG16L1 (S278)
75 kDa
ATG16L1
75 kDa
pNF-κB (S536)
75 kDa
NF-κB
135 kDa
ULK1
100 kDa
IKKα
135 kDa
Vinculin
pATG16L1 / ATG16L1 (fold increase)
n.s p=0.19
p=5.5E-3
n.s p=0.10
p=2.0E-3
NT
-AA
TNFα (20 ng/mL)
TNFα (50 ng/mL)
WT
ULK1/2 dKO
IKKα KO
D
Infected cells(%)
n.s p=0.43
n.s p=0.81
WT
ULK1/2 dKO
IKKα KO
E
WT
IKKα KO
ULK1/2 dKO
External LPS
Total LPS
LC3B
Merge
F
LC3B-positive bacteria(%)
n.s p=0.15
p=1.8E-2
WT
ULK1/2 dKO
IKKα KO

EV3.

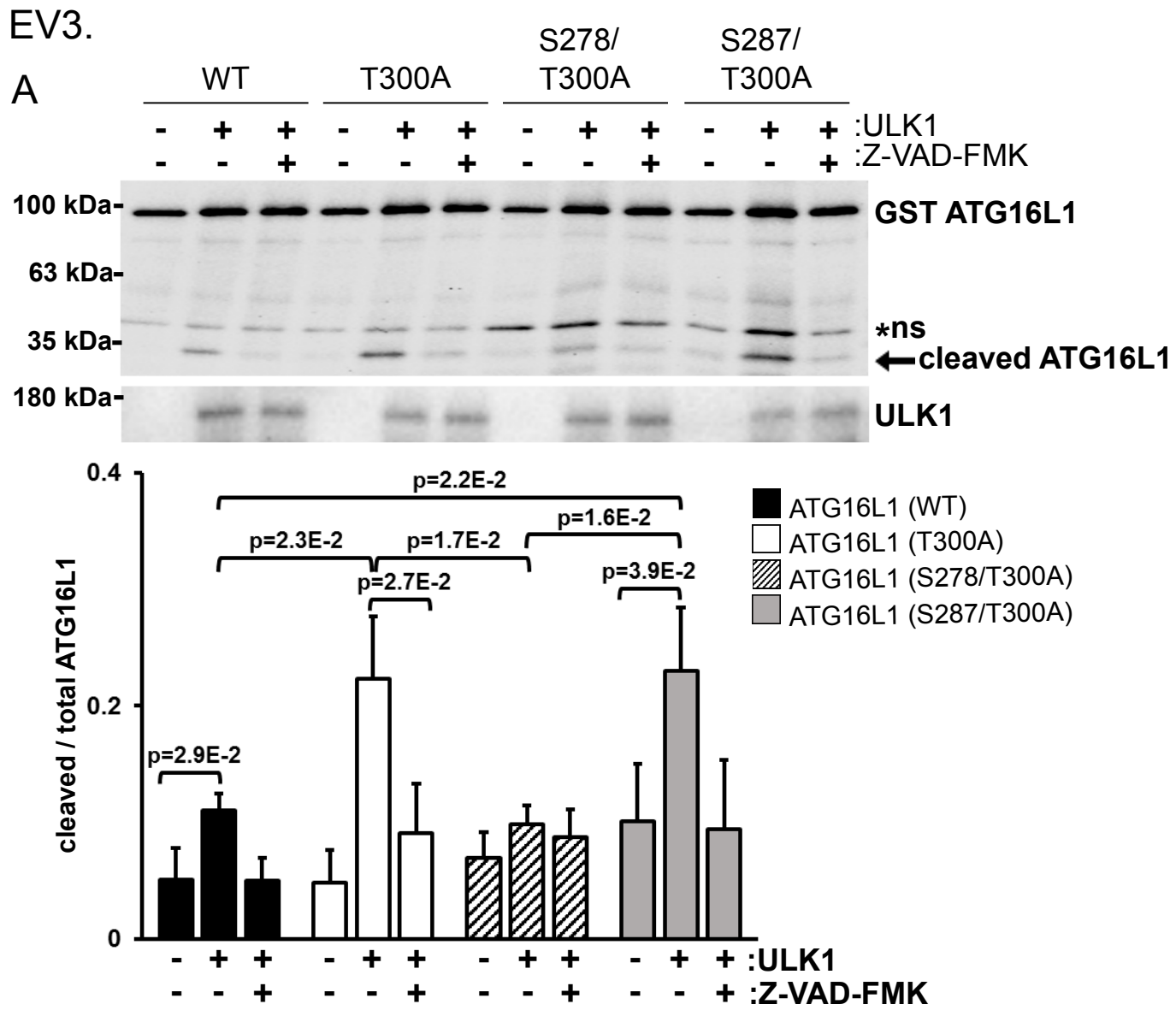

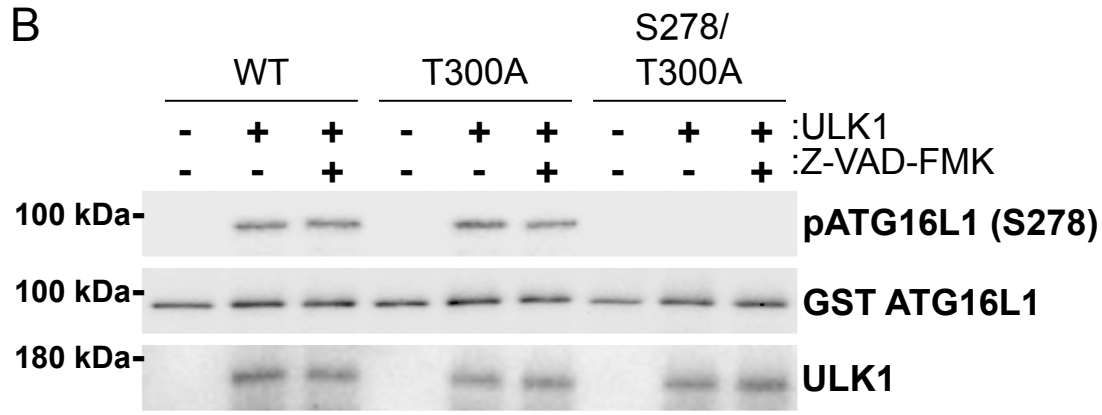

C

Gene	Cell	Disruption of exon 1 of ATG16L1	
ATG16L1	HCT116	WT: tgacttcccc cgctggaagc.....ttcgaggaga A1/A2: tgacttcccc cg--------.....-tcgaggaga	59bp del.
	HEK293A	WT: tgacttcccc cgctggaagc.....ttcgaggaga A1: tgacttcccc cg-tggaagc.....ttcgaggaga A2: tgacttcccc cg--------.....-ttcgaggaga	1 bp del. 58 bp del.

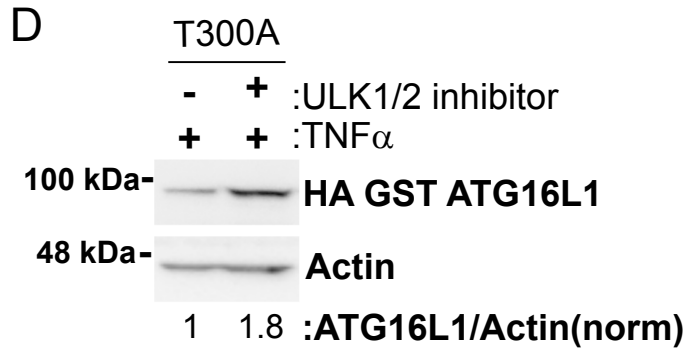

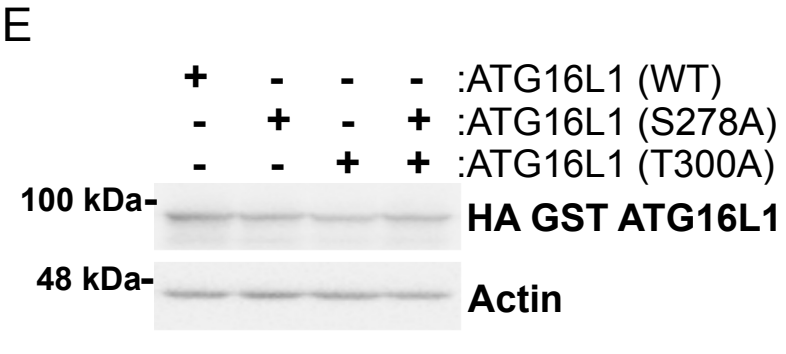

EV4

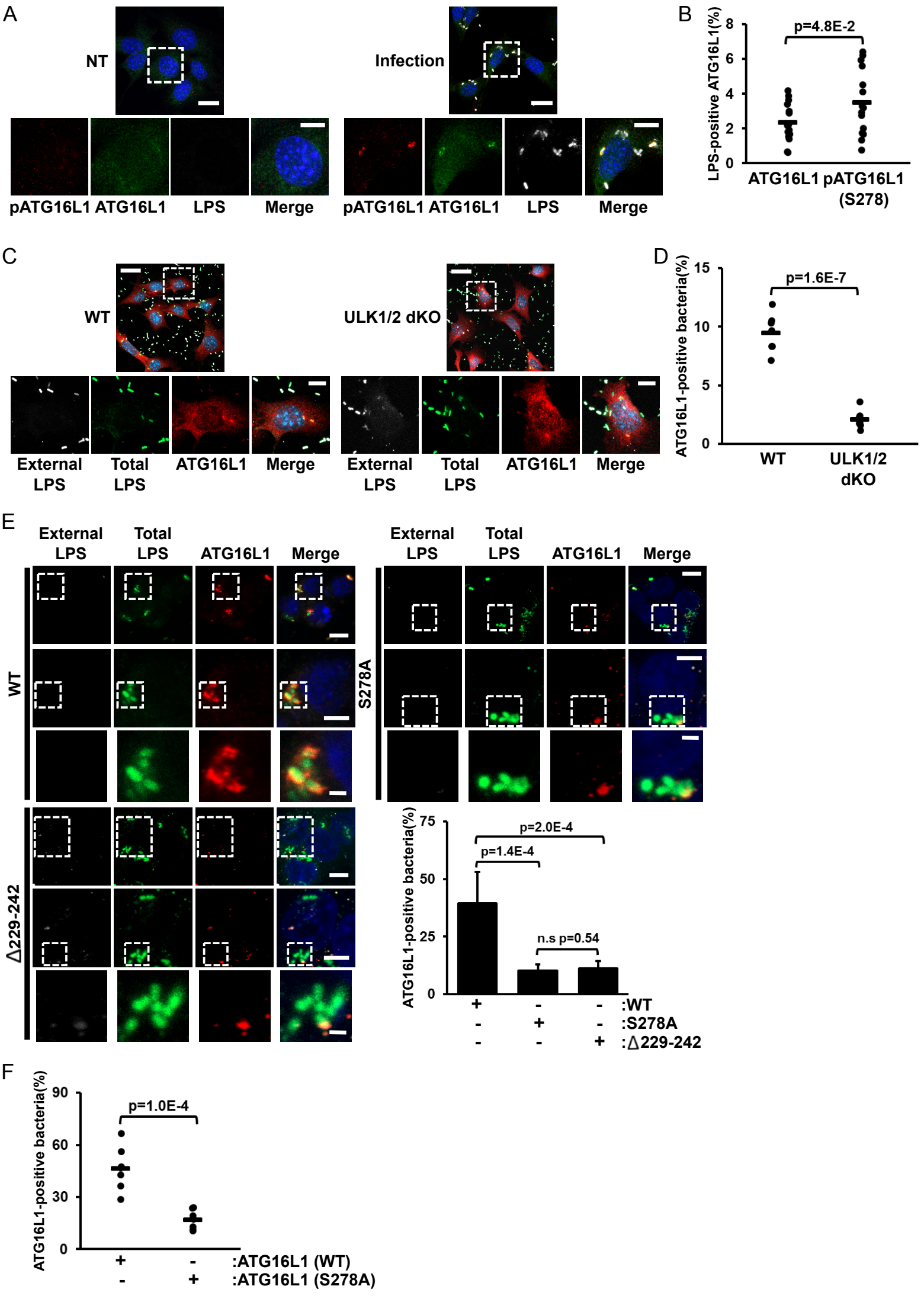
A
NT
Infection
pATG16L1
ATG16L1
LPS
Merge
B
LPS-positive ATG16L1(%)
p=4.8E-2
ATG16L1
pATG16L1 (S278)
C
WT
ULK1/2 dKO
External LPS
Total LPS
ATG16L1
Merge
D
ATG16L1-positive bacteria(%)
p=1.6E-7
WT
ULK1/2 dKO
E
WT
S278A
Δ229-242
p=2.0E-4
p=1.4E-4
n.s p=0.54
:WT
:S278A
:Δ229-242
F
p=1.0E-4
:ATG16L1 (WT)
:ATG16L1 (S278A)

EV5.

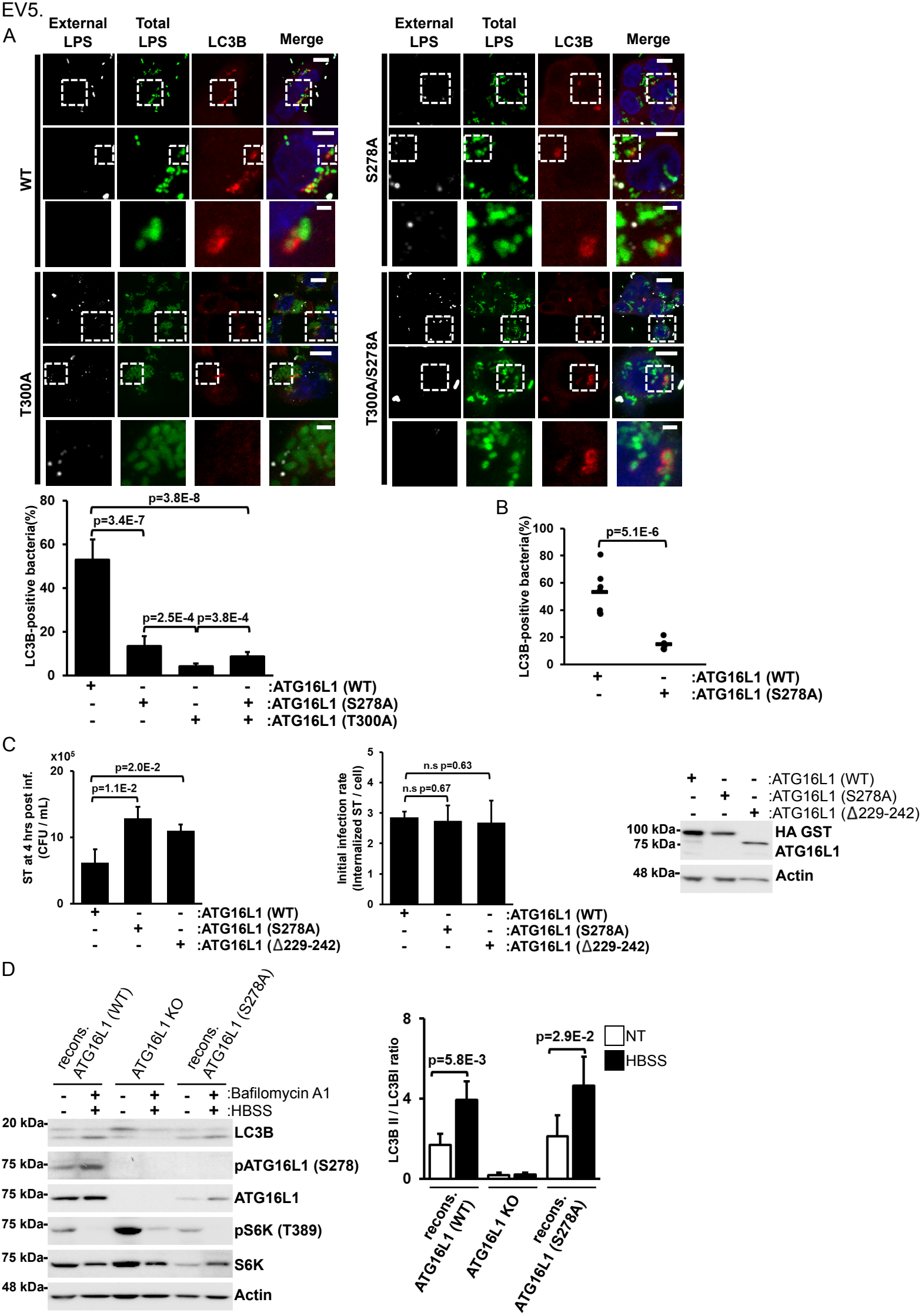
A
External LPS
Total LPS
LC3B
Merge
WT
S278A
T300A
T300A/S278A
LC3B-positive bacteria(%)
p=3.8E-8
p=3.4E-7
p=2.5E-4
p=3.8E-4
:ATG16L1 (WT)
:ATG16L1 (S278A)
:ATG16L1 (T300A)
B
p=5.1E-6
C
ST at 4 hrs post inf. (CFU / mL)
p=2.0E-2
p=1.1E-2
Initial infection rate (Internalized ST / cell)
n.s p=0.63
n.s p=0.67
:ATG16L1 (Δ229-242)
100 kDa-
75 kDa-
HA GST
ATG16L1
48 kDa-
Actin
D
recons. ATG16L1 (WT)
ATG16L1 KO
recons. ATG16L1 (S278A)
:Bafilomycin A1
:HBSS
20 kDa-
LC3B
75 kDa-
pATG16L1 (S278)
ATG16L1
pS6K (T389)
S6K
LC3B II / LC3BI ratio
p=5.8E-3
p=2.9E-2
NT
HBSS